

Remedying Target-Domain Astigmatism for Cross-Domain Few-Shot Object Detection

Yongwei Jiang Yixiong Zou* Yuhua Li Ruixuan Li

School of Computer Science and Technology, Huazhong University of Science and Technology

{jiangyongwei, yixiong, idcliyuhua, rxli}@hust.edu.cn

Abstract

Cross-domain few-shot object detection (CD-FSOD) aims to adapt pretrained detectors from a source domain to target domains with limited annotations, suffering from severe domain shifts and data scarcity problems. In this work, we find a previously overlooked phenomenon: models exhibit dispersed and unfocused attention in target domains, leading to imprecise localization and redundant predictions, just like a human cannot focus on visual objects. Therefore, we call it the target-domain **Astigmatism** problem. Analysis on attention distances across transformer layers reveals that regular fine-tuning inherently shows a trend to remedy this problem, but results are still far from satisfactory, which we aim to enhance in this paper. Biologically inspired by the human fovea-style visual system, we enhance the fine-tuning’s inherent trend through a center-periphery attention refinement framework, which contains (1) a Positive Pattern Refinement module to reshape attention toward semantic objects using class-specific prototypes, simulating the visual center region; (2) a Negative Context Modulation module to enhance boundary discrimination by modeling background context, simulating the visual periphery region; and (3) a Textual Semantic Alignment module to strengthen center-periphery distinction through cross-modal cues. Our bio-inspired approach transforms astigmatic attention into focused patterns, substantially improving adaptation to target domains. Experiments on six challenging CD-FSOD benchmarks consistently demonstrate improved detection accuracy and establish new state-of-the-art results.

1. Introduction

Great progress has been made in object detection [2, 4, 27], thanks to the development of pretrained models on large-scale general data. However, real-world applications always require generalizing pretrained models to downstream expert domains, such as medical diagnosis [1, 24] and in-

*Corresponding author.

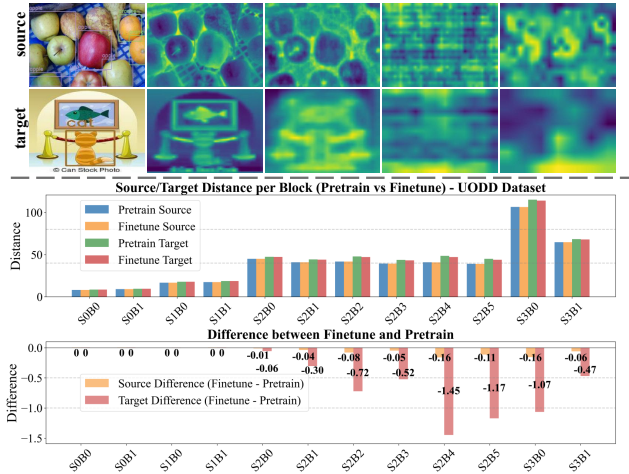


Figure 1. Visualization and quantification of the target-domain **Astigmatism** problem. **Top:** Attention maps measured across transformer blocks show that, in source domains (first row), attention progressively focuses on foreground objects, while in target domains (second row), attention remains persistently dispersed, resulting in oversized boxes and redundant predictions in object detection. **Bottom:** Attention distance across network depth (S_xB_y denotes Stage x , Block y in the Swin Transformer) reveals: (1) a observed rise-then-fall trend in attention distance, reflecting an initial broad attention that gradually concentrates on objects for precise localization; (2) consistently higher attention dispersion in target domains compared to source domains; and (3) regular fine-tuning only marginally reduces this attention dispersion.

dustrial inspection [44], where sufficient training samples are hard to collect, making it difficult to adapt the pretrained model. To address this issue, the cross-domain few-shot object detection (CD-FSOD) [5] task has been proposed, which aims to pretrain an object detection model on a source-domain dataset and then adapt it to target domains with only scarce training data. The domain gap and data scarcity have made it a challenging and unsolved problem.

Existing CD-FSOD approaches have explored various techniques, including distillation-based methods [33] and

domain-adaptive optimization strategies [5, 7]. However, the attention of detection models across different domains is rarely studied. To delve into it, we conduct an in-depth analysis of the model’s attention across transformer blocks and discover an interesting phenomenon (Fig. 1 top): the model experiences **Astigmatism** on target domains. That is, in source domains, attention progressively concentrates on foreground objects as network depth increases, especially at the last two blocks. By contrast, in target domains, attention remains dispersed and unfocused, leading to oversized bounding boxes and redundant predictions for object detection, just like a human not knowing what to focus on in a new domain and just coarsely looking at the image.

To quantify this phenomenon, we measure the attention distance [21] of each layer in the encoder as $\bar{d} = \frac{1}{N} \sum_{i=1}^N \sum_{j=1}^N A_{ij} \cdot ||p_i - p_j||$, where A_{ij} represents attention weights between tokens, and p_i and p_j denote spatial positions, e.g., (0, 0) or (14, 14). As shown in Fig. 1 bottom, we find that: (1) The attention distance follows a rise-then-fall trend with the network depth growing, indicating the learned patterns grow from local to global and finally return to focused ones for accurate localization. (2) Target domains consistently show higher attention distance than source domains, indicating dispersed attention and ineffective feature extraction. (3) Regular finetuning consistently tries to reduce this dispersion, but can only marginally achieve this goal, as the *Target Differences* are all negative, but the *Finetune Targets* are still higher than *Finetune Sources* in Fig. 1 bottom. These results validate that Astigmatism widely exists in CD-FSOD, and the model inherently tries to remedy this problem via regular finetuning. However, due to domain gaps and data scarcity, results are still far from satisfactory.

In this paper, we aim to enhance the model’s inherent trend in remedying the Astigmatism problem, helping the model develop a concentrated attention on the semantic object for CD-FSOD. To handle this human-like problem, we also take inspiration from human visual systems. As shown in Fig. 2, humans possess a fovea-style visual system, where the center perception zone is dedicated to capturing highly detailed visual information, while the peripheral zones capture less details [13, 31]. Such a center-peripheral visual property keeps human attention concentrated on the center zone [26]. Biologically inspired by this center-peripheral property of human visual systems, we design three complementary modules to enhance the representation of both the core and peripheral perception zones, and strengthen the contrast of these zones. Specifically, we design a Positive Pattern Refinement module that reshapes attention toward foreground objects by leveraging class-specific prototypes (central region); a Negative Context Modulation module that enhances object-background boundaries by explicitly modelling background contexts (peripheral region);

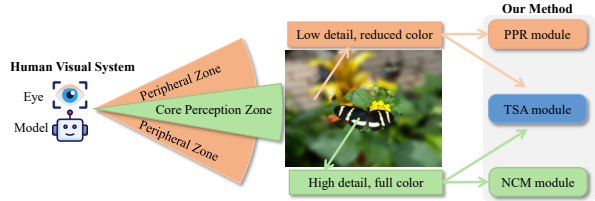


Figure 2. The inspiration from human fovea-style vision to remedy the Astigmatism problem. Our method mimics the human visual system: the Core Perception Zone (green) with high-detail processing guides the Positive Pattern Refinement (PPR) module to reshape attention more effectively toward foreground objects, while the Peripheral Zone (orange) with reduced details informs the Negative Context Modulation (NCM) module to enhance object-background boundaries by modeling background contexts. The Textual Semantic Alignment (TSA) module enforces the distinctions between center and peripheral regions, analogous to the center-surround mechanism of biological perception.

and a Textual Semantic Alignment mechanism that enforces these distinctions through cross-modal knowledge integration using “not [class]” descriptors (e.g., “not sofa, not dog”) to establish clearer foreground-background separation. This multi-faceted approach effectively transforms the astigmatic attention patterns in target domains into focused ones, improving target-domain performance. In summary:

- To the best of our knowledge, we are the first to find the target-domain Astigmatism problem, where the model exhibits dispersed attention that is harmful for object detection. Though the model tries to remedy it through the regular finetuning, the result is still far from satisfactory.
- Inspired by the human visual system, we propose a center-peripheral prototype-based method to enhance the model’s inherent trend in remedying the Astigmatism problem, containing a Positive Pattern Refinement (PPR) module, a Negative Context Modulation (NCM) module, and a Textual Semantic Alignment (TSA) module.
- In the PPR module, we design to leverage class-specific prototypes to enhance the visual center region for the foreground attention. In the NCM module, we model background contexts for enhancing the visual peripheral region. In the TSA module, we strengthen the distinctions between center and peripheral regions through cross-modal knowledge integration.
- We demonstrate consistent performance improvements across six challenging cross-domain datasets, establishing new state-of-the-art results in the CD-FSOD task.

2. Related Work

2.1. Cross-Domain Few-Shot Object Detection

Cross-Domain Few-Shot Object Detection (CD-FSOD) seeks to effectively tackle the dual challenges of domain

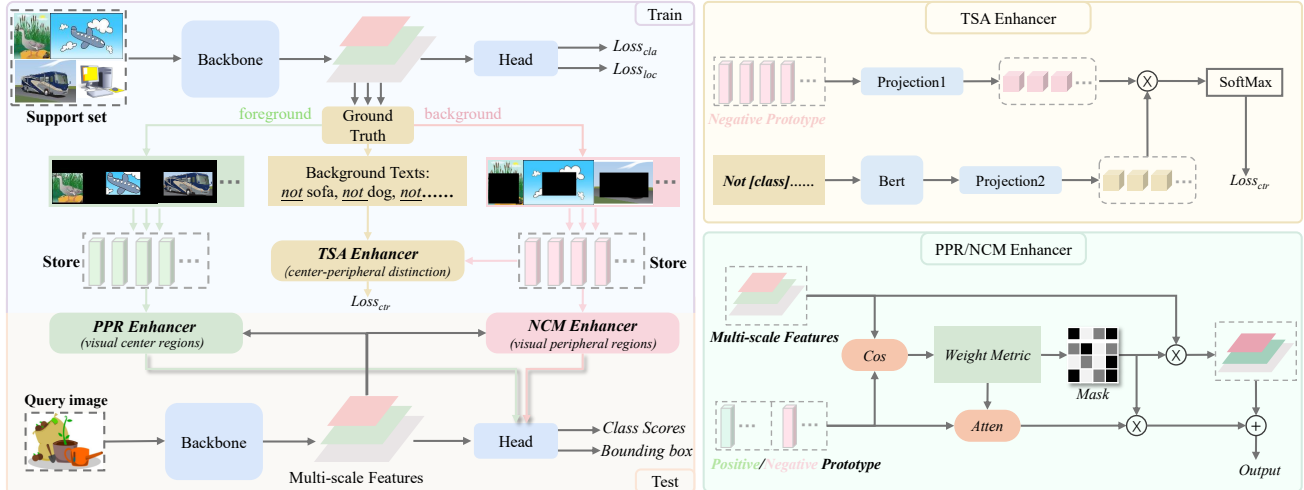


Figure 3. Overview of our human-vision-inspired framework to remedy the Astigmatism problem in CD-FSOD. The architecture integrates three complementary modules: (1) Positive Pattern Refinement (PPR) reshapes attention toward foreground objects using class prototypes; (2) Negative Context Modulation (NCM) enhances object-background boundaries through explicit background modeling; and (3) Textual Semantic Alignment (TSA) enhances these distinctions via cross-modal knowledge integration with negative descriptors (“not [class]”). During training (top), the model is optimized with both detection and alignment objectives, and extracts discriminative prototypes from support examples, stored in positive and negative repositories. At inference (bottom), stored prototypes turn dispersed attention patterns in query images into crystallized object-centric representations, analogous to the human center-peripheral visual system.

shift and data scarcity [41, 43, 47–51]. Early works tackled these issues separately—FAFR-CNN [28] introduced domain-adaptive detection with limited examples via pairing, while PICA [45] explored instance-level feature alignment. DAPN [42] attempts to unify few-shot learning and domain adaptation within a joint framework. Related efforts such as AcroFOD [6] applies augmentation in broader cross-domain settings. Additional methods like SDAFL [23] and FUM [34] explore domain-specific modalities and uncertainty modeling. Integrated approaches followed, with MoF-SOD [9] analyzing architecture effects on generalization, Distill-CDFSOD [33] using knowledge distillation to retain source priors, and CD-ViTO [5] establishing benchmarks across diverse domains. Unlike prior work [11, 37–40], we tackle the underexplored issue of cross-domain attention dispersion, improving knowledge transfer under diverse categories and visual shifts in few-shot settings.

2.2. Context Modeling and Feature Transformation

Recent works have emphasized contextual information patterns as key for visual understanding tasks. Approaches like Dual Semantic Guidance [30] use background screening modules to filter irrelevant visual information, while CD-Former [20] tackles feature confusion via explicit object-background distinguishing mechanisms. For domain adaptation, IPNet [35] develops separate foreground and background domain alignment paths with specialized discriminators. Beyond detection, DualAnoDiff [12] uses background cues for content consistency within surrounding contexts in anomaly detection, while NegativePrompt [29] studies how negative contextual elements shape model per-

formance in language domains. These methods overlook the distinctive cross-domain feature dispersion phenomenon that we reveal, and fail to exploit negative contextual cues for enhancing cross-modal representations.

3. Method

In this section, we introduce our bio-inspired approach for remedying the Astigmatism problem in CD-FSOD. As illustrated in Figure 3, our framework integrates Positive Pattern Refinement (PPR) to reshape attention toward foreground objects, working alongside Negative Context Modulation (NCM) which enhances object-background boundaries. Complementing these, Textual Semantic Alignment (TSA) enhances distinctions via cross-modal knowledge.

3.1. Preliminaries

Cross-Domain Few-Shot Object Detection (CD-FSOD)

adapts a model trained on a source domain with abundant labeled data (typically COCO [18]) to a target domain $\mathcal{D}_T = \{(I_i^T, \mathcal{B}_i^T, \mathcal{C}_i^T)\}_{i=1}^{N_T}$ with sparse annotations and domain gap. Here, I_i represents images, \mathcal{B}_i denotes bounding boxes, and \mathcal{C}_i indicates class labels. The model is first trained on the source domain, then fine-tuned using a compact support set $\mathcal{S} = \{(I_i^T, \mathcal{B}_i^T, \mathcal{C}_i^T)\}_{i=1}^{N \times K}$ containing exactly K annotated examples for each of the N novel classes. Finally, the model is evaluated on previously unseen target domain images from the query set \mathcal{Q} . In this paper, we solely focus on the fine-tuning stage in the target domain.

Grounded Language-Image Pre-training (GLIP)

serves as our baseline model for object detection. Given

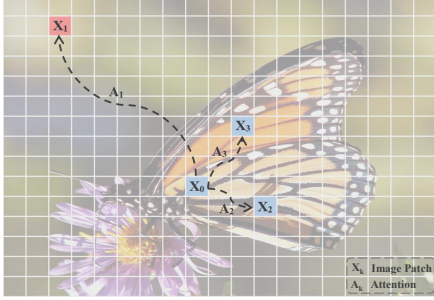


Figure 4. Attention distribution around a foreground patch x_0 . Dashed arrows labeled A_k indicate attention from x_0 to neighbors x_k . Same-object neighbors x_2, x_3 are spatially near and should receive high attention, whereas the background patch x_1 is distant and should be weak. In target-domain Astigmatism, domain shift diverts attention toward the distant background ($A_1 \uparrow$; $A_2, A_3 \downarrow$), yielding dispersed attention and a larger attention distance. Since the spatial distance between patches are fixed, our method reverses this dispersion by (i) down-weighting background responses A_1 via a learned background prototype and simple “not [class]” cues (NCM/TSA module) to suppress spurious foreground–background affinity, and (ii) up-weighting same-object responses A_2, A_3 via class-specific foreground prototypes (PPR module) to strengthen intra-object compatibility, thereby shortening attention distance and restoring a focused, object-centric pattern.

an input image I , GLIP extracts visual features through a backbone: $\mathbf{F}_v = \{\mathbf{f}_v^1, \mathbf{f}_v^2, \dots, \mathbf{f}_v^L\} = \text{Backbone}(I)$, where \mathbf{F}_v represents the set of multi-scale visual features at L different scales, and \mathbf{f}_v^s denotes the feature map at scale s . For text inputs, GLIP employs BERT to process queries, yielding textual features \mathbf{F}_t . The model subsequently employs a fusion mechanism that combines these representations: $\mathbf{F}_{fused} = \text{DynamicConv}(\mathbf{F}_v, \mathbf{F}_t)$. These fused features are then fed into detection heads to produce class logits and corresponding bounding box predictions. The baseline detection loss is therefore formulated as:

$$\mathcal{L}_{detection} = \mathcal{L}_{cls} + \mathcal{L}_{loc} \quad (1)$$

where \mathcal{L}_{cls} and \mathcal{L}_{loc} represent classification and localization losses, respectively.

3.2. How to reduce attention distance to avoid Astigmatism?

In Fig. 1, we validate the Astigmatism problem by measuring the attention distance. In this section, we aim to reduce such distances to avoid Astigmatism. Take a foreground patch x_0 as an example (Fig. 4), suppose it attends to $\{x_k\}$, let A_k denote the attention from x_0 to x_k , p_k is their spatial positions, and $r_k = \|p_0 - p_k\|$ is the spatial distances, the attention distance is calculated as

$$d(x_0) = \sum_k A_k r_k. \quad (2)$$

For illustration (*without loss of generality*), consider one background neighbor x_1 and two same-object neighbors

x_2, x_3 (omitting heads, batch indices, etc.), which leads to

$$d(x_0) = A_1 r_1 + A_2 r_2 + A_3 r_3. \quad (3)$$

In target domains, we consistently observe larger attention distances (Fig. 1). Domain shift induces *foreground–background confusion*: the distant background neighbor x_1 collects more attention ($A_1 \uparrow$) while the attention to same-object neighbors x_2, x_3 shrinks ($A_2, A_3 \downarrow$). With fixed spatial offsets r_k and $r_1 > r_2, r_3$, this attention distribution necessarily increases $d(x_0)$, manifesting dispersed, target-domain attention (Astigmatism).

Therefore, to avoid Astigmatism, we need to rectify the attention distribution so that patches within the same object possess higher attention. Our modules reallocate $\{A_k\}$ in a complementary way: (i) **PPR** uses class-specific foreground prototypes to strengthen same-object similarity and continuity along the object extent, increasing A_2, A_3 ; (ii) **NCM** builds a unified background prototype to enhance the representation of background, reducing its confusion with foreground and decreasing A_1 ; and (iii) **TSA** employs simple prompts “not [class]” to sharpen foreground–background separation via cross-modal alignment, further decreasing A_1 and stabilizing gains on A_2, A_3 .

3.3. Positive Pattern Refinement

Based on the above analysis, we first design a Positive Pattern Refinement (PPR) module that uses class-specific prototypes from support examples to enhance foreground features, simulating the center region of human vision.

For clarity and simplicity, we present our method using single-scale notation, while our framework processes multi-scale features as shown in Figure 3. During the finetuning phase, foreground prototypes are computed as:

$$\mathbf{p}_{fg}^c = \frac{1}{|\mathcal{B}_{fg}^c|} \sum_{(x,y) \in \mathcal{B}_{fg}^c} \mathbf{f}_v(x, y) \quad (4)$$

where \mathcal{B}_{fg}^c denotes the set of pixel coordinates within foreground regions of class c . Each prototype $\mathbf{p}_{fg}^c \in \mathbb{R}^{1 \times 1 \times D}$ represents the averaged feature representation for class c , where D is the feature dimension. These prototypes are stored in \mathcal{P}_{fg} to capture target object characteristics.

During inference, we first compute cosine similarity between each feature map position and stored prototypes:

$$\text{sim}(\mathbf{f}_v(x, y), \mathbf{p}_{fg}^c) = \frac{\mathbf{f}_v(x, y) \cdot \mathbf{p}_{fg}^c}{\|\mathbf{f}_v(x, y)\|_2 \cdot \|\mathbf{p}_{fg}^c\|_2 + \epsilon} \quad (5)$$

where $\mathbf{f}_v(x, y) \in \mathbb{R}^{1 \times 1 \times D}$ represents the feature vector at position (x, y) in the feature map, $\|\cdot\|_2$ denotes the L2 norm, and $\epsilon = 10^{-8}$ ensures numerical stability.

We compute metrics via temperature-scaled softmax: $w_c(x, y) = \text{softmax}(\text{sim}(\mathbf{f}_v(x, y), \mathbf{p}_{fg}^c)/T)$. In parallel, we

Table 1. 1-shot cross-domain detection performance comparison (mAP). [†] indicates results reported in CD-ViTO [5]. Methods with * are reimplemented by us using Swin-Tiny backbone. GLIP and our method are also implemented with Swin-Tiny backbone.

Method	Backbone	Venue	ArTaxOr	Clipart1k	DIOR	DeepFish	NEU-DET	UODD	Avg.
Distill [†] [32]	ResNet50	ICASSP'23	5.10	7.60	10.50	–	–	5.90	/
ViTDet [†] [16]	ViT-B/14	ECCV'22	5.90	6.10	12.90	0.90	2.40	4.00	5.37
ViTDet* [16]	Swin-T	ECCV'22	8.85	10.22	18.50	1.06	4.54	4.90	8.01
Detic [†] [46]	ViT-L/14	ECCV'22	3.20	15.10	4.10	9.00	3.80	4.20	6.57
Detic* [46]	Swin-T	ECCV'22	4.45	19.22	5.70	10.49	7.15	5.12	8.69
DE-ViT [†] [36]	ViT-L/14	arXiv'23	10.50	13.00	14.70	19.30	0.60	2.40	10.08
DE-ViT* [36]	Swin-T	arXiv'23	14.81	16.06	18.00	22.40	1.20	2.97	12.57
GLIP [15]	Swin-T	CVPR'22	21.40	33.35	19.09	27.23	8.84	3.99	18.98
CD-ViTO [†] [5]	ViT-L/14	ECCV'24	21.00	17.70	17.80	20.30	3.60	3.10	13.92
CD-ViTO* [5]	Swin-T	ECCV'24	20.85	21.83	18.90	23.53	6.82	3.85	15.96
Domain-RAG* [17]	Swin-T	NIPS'25	21.47	22.53	18.97	24.67	7.53	3.92	16.52
VFM-MoE* [19]	Swin-T	NIPS'25	23.38	25.67	19.03	25.45	8.12	3.87	17.59
Ours	Swin-T	–	27.93	38.75	25.67	30.43	12.88	7.18	23.81

Table 2. 5-shot cross-domain detection performance comparison (mAP). [†] indicates results reported in CD-ViTO [5]. Methods with * are reimplemented by us using Swin-Tiny backbone. GLIP and our method are also implemented with Swin-Tiny backbone.

Method	Backbone	Venue	ArTaxOr	Clipart1k	DIOR	DeepFish	NEU-DET	UODD	Avg.
Distill [†] [32]	ResNet50	ICASSP'23	12.50	23.30	19.10	15.50	16.00	12.20	16.43
ViTDet [†] [16]	ViT-B/14	ECCV'22	20.90	23.30	23.30	9.00	13.50	11.10	16.85
ViTDet* [16]	Swin-T	ECCV'22	21.05	23.45	23.45	11.03	19.96	15.07	19.00
Detic [†] [46]	ViT-L/14	ECCV'22	8.70	20.20	12.10	14.30	14.10	10.40	13.30
Detic* [46]	Swin-T	ECCV'22	10.63	20.31	14.78	17.46	20.80	14.07	16.34
DE-ViT [†] [36]	ViT-L/14	arXiv'23	38.00	38.10	23.40	21.20	7.80	5.00	22.25
DE-ViT* [36]	Swin-T	arXiv'23	38.15	38.27	23.52	25.89	11.50	6.79	24.02
GLIP [15]	Swin-T	CVPR'22	49.11	39.28	28.39	28.40	19.55	11.40	29.36
CD-ViTO [†] [5]	ViT-L/14	ECCV'24	47.90	41.10	26.90	22.30	11.40	6.80	26.07
CD-ViTO* [5]	Swin-T	ECCV'24	48.12	40.28	27.05	28.26	16.84	9.24	28.30
Domain-RAG* [17]	Swin-T	NIPS'25	46.13	41.47	25.23	27.67	17.53	9.87	27.98
VFM-MoE* [19]	Swin-T	NIPS'25	48.23	39.13	26.34	27.58	18.67	10.73	28.45
Ours	Swin-T	–	54.98	44.83	29.41	33.87	23.64	15.66	33.73

use a binary mask to flag high-similarity prototypes.

$$\mathbf{M}_{fg}(x, y) = \begin{cases} 1, & \text{if } \max_c \text{sim}(\mathbf{f}_v(x, y), \mathbf{P}_{fg}^c) > \tau_{fg} \\ 0, & \text{otherwise} \end{cases} \quad (6)$$

where τ_{fg} serves as the similarity threshold. With this mask and weight metrics, we apply targeted feature enhancement:

$$\mathbf{f}_v^{\text{pos}}(x, y) = \mathbf{f}_v(x, y) \cdot \mathbf{M}_{fg}(x, y) + \gamma_{fg} \sum_c w_c(x, y) \mathbf{P}_{fg}^c \cdot \mathbf{M}_{fg}(x, y) \quad (7)$$

where γ_{fg} controls the strength of prototype contribution. This selective approach ensures enhancement occurs precisely where objects of interest are likely to be present, effectively reshaping dispersed attention patterns into focused object-centric representations in target domains.

3.4. Negative Context Modulation

While foreground refinement is crucial, effective object detection equally depends on proper background modeling. Our NCM module complements the foreground focus by modeling contextual elements outside object regions, mimicking the peripheral region of human visual systems.

During the finetuning phase, we construct a unified background prototype from regions outside ground truth boxes:

$$\mathbf{P}_{bg} = \frac{1}{|\mathcal{B}_{bg}|} \sum_{(x, y) \in \mathcal{B}_{bg}} \mathbf{f}_v(x, y) \quad (8)$$

where background regions \mathcal{B}_{bg} are identified as:

$$\mathcal{B}_{bg} = \{(x, y) | (x, y) \notin \bigcup_{b \in \mathcal{B}_{gt}} b\} \quad (9)$$

with \mathcal{B}_{gt} denoting all ground truth boxes in the support set.

During the inference phase, following the same pipeline as PPR, we apply background-aware feature modulation:

$$\mathbf{f}_v^{\text{neg}}(x, y) = \mathbf{f}_v(x, y) \cdot \mathbf{M}_{bg}(x, y) + \gamma_{bg} \mathbf{P}_{bg} \cdot \mathbf{M}_{bg}(x, y) \quad (10)$$

where $\mathbf{M}_{bg}(x, y)$ is computed using the same similarity-based thresholding as in PPR, and γ_{bg} controls background contribution. Unlike the class-specific strategy in PPR, background is treated as a unified concept, enabling better separation of foreground and context in novel domains.

3.5. Textual Semantic Alignment

Beyond visual feature refinement, leveraging semantic knowledge can further enhance domain adaptation. Our

Table 3. 10-shot cross-domain detection performance comparison (mAP). † indicates results reported in CD-ViTO [5]. Methods with * are reimplemented by us using Swin-Tiny backbone. GLIP and our method are also implemented with Swin-Tiny backbone.

Method	Backbone	Venue	ArTaxOr	Clipart1k	DIOR	DeepFish	NEU-DET	UODD	Avg.
Distill† [32]	ResNet50	ICASSP’23	18.10	27.30	26.50	15.50	21.10	14.50	20.50
ViTDet† [16]	ViT-B/14	ECCV’22	23.40	25.60	29.40	6.50	15.80	15.60	19.38
ViTDet* [16]	Swin-T	ECCV’22	24.20	25.93	30.10	8.04	22.52	19.55	21.72
Detic† [46]	ViT-L/14	ECCV’22	12.00	22.30	15.40	17.90	16.80	14.40	16.47
Detic* [46]	Swin-T	ECCV’22	13.80	22.59	17.20	22.04	23.97	16.58	19.36
DE-ViT† [36]	ViT-L/14	arXiv’23	49.20	40.80	25.60	21.30	8.80	5.40	25.18
DE-ViT* [36]	Swin-T	arXiv’23	50.50	41.28	26.80	26.23	12.60	13.72	28.52
GLIP [15]	Swin-T	CVPR’22	62.01	41.04	31.10	29.29	20.56	19.56	33.93
CD-ViTO† [5]	ViT-L/14	ECCV’24	60.50	44.30	30.80	22.30	12.80	7.00	29.62
CD-ViTO* [5]	Swin-T	ECCV’24	62.30	43.83	31.15	27.46	18.26	17.84	33.47
Domain-RAG* [17]	Swin-T	NIPS’25	59.87	42.85	29.23	28.67	18.87	17.93	32.81
VFM-MoE* [19]	Swin-T	NIPS’25	63.13	41.23	30.67	29.13	20.23	19.23	33.94
Ours	Swin-T	–	68.40	47.63	34.25	35.58	24.96	24.18	39.17

Table 4. Summary of target datasets used in our evaluation.

Dataset	Classes	Images	Boxes	Domain	Challenge
ArTaxOr	7	1383	1628	photorealistic	small objects
Clipart1k	20	500	1526	cartoon	style abstraction
DIOR	20	5000	28810	aerial	medium-scale
DeepFish	1	909	3029	aquatic	poor visibility
NEU-DET	6	360	834	industrial	subtle features
UODD	3	506	3218	underwater	complex clutter

Textual Semantic Alignment (TSA) module enhances object-background distinctions via cross-modal knowledge.

For each target domain, we encode negative class concepts using “not [class]” descriptors and utilize the background prototype from NCM as the visual representation:

$$\mathbf{F}_t^{bg} = \text{BERT}(\mathcal{T}_{bg}), \quad \mathbf{F}_v^{bg} = \mathbf{p}_{bg} \quad (11)$$

where \mathcal{T}_{bg} represents text prompts like “not sofa, not dog” corresponding to target classes. Importantly, all background texts employ **simple prompts** derived from dataset categories, which we describe in detail in the Appendix.

These visual and textual representations are aligned through projection into a shared semantic space:

$$\mathcal{S} = \text{Proj}_1(\mathbf{F}_v^{bg}) \cdot \text{Proj}_2(\mathbf{F}_t^{bg})^T \quad (12)$$

where Proj_1 and Proj_2 are learnable projection layers, and \cdot denotes matrix multiplication.

We optimize the alignment to maximize similarity between visual and textual background features:

$$\mathcal{L}_{ctr} = -\log \frac{\exp(\text{diag}(\mathcal{S})/\tau)}{\sum_{i,j} \exp(\mathcal{S}_{i,j}/\tau)} \quad (13)$$

where τ is a temperature parameter. This formulation maximizes the diagonal elements (positive pairs) while minimizing off-diagonal ones (negative pairs). This cross-modal alignment offers extra supervision to remedy attention dispersion by creating clearer object-background boundaries.

3.6. Model Training and Testing

Our framework operates differently during finetuning and inference phases, as illustrated in Figure 3. The integra-

tion of our three complementary modules follows a coordinated architecture that remedies the Astigmatism problem through targeted feature transformation.

During finetuning, we first extract class-specific foreground prototypes and unified background prototypes from support examples. The model is then optimized with both detection and cross-modal alignment objectives:

$$\mathcal{L}_{total} = \mathcal{L}_{detection} + \lambda_{bg} \cdot \mathcal{L}_{ctr} \quad (14)$$

where λ_{bg} balances detection and alignment objectives.

During inference, we apply the prototype-based enhancement through both PPR and NCM enhancers. To avoid potential conflicts between positive and negative enhancements, we use a complementary fusion strategy:

$$\mathbf{F}_v^{\text{enhanced}} = \mathbf{f}_v^{\text{pos}} + \mathbf{f}_v^{\text{neg}} \quad (15)$$

where $\mathbf{f}_v^{\text{pos}}$ and $\mathbf{f}_v^{\text{neg}}$ denote positive and negative enhanced features derived from similarities, enabling flexible regional enhancement. The enhanced features $\mathbf{F}_v^{\text{enhanced}}$ are then fed into the baseline detection heads for class and box prediction. This dual-pathway design enhances foreground features while preserving object-background boundaries, turning dispersed attention into focused representations and alleviating the astigmatism problem in CD-FSOD.

4. Experiments

4.1. Dataset and Metrics

Our evaluation spans six cross-domain datasets (Table 4): ArTaxOr [3] (photorealistic arthropods, small objects), Clipart1k [8] (cartoon abstractions), DIOR [14] (aerial, medium-scale), DeepFish [22] (underwater visibility), NEU-DET [25] (industrial defects, imbalance), and UODD [10] (underwater organisms, complex, imbalanced). We report COCO-style mAP over IoU 0.5–0.95.

4.2. Benchmark Comparisons

Tables 1, 2, and 3 show our method consistently surpasses prior work in mAP across all few-shot settings. For fairness, methods marked * are reimplemented with Swin-Tiny. We

Table 5. Ablation study showing each component’s contribution to overall performance (mAP %) in 5-shot setting.

Components				Datasets						
NCM	PPR	TSA		ArTaxOr	Clipart1k	DIOR	DeepFish	NEU-DET	UODD	
✓				48.11	39.28	27.39	28.40	19.55	11.40	
✓	✓			49.95	40.52	27.75	29.58	20.48	12.21	
✓	✓	✓		52.68	42.95	28.62	31.96	22.38	14.26	
✓	✓	✓		54.98	44.83	29.41	33.87	23.64	15.66	

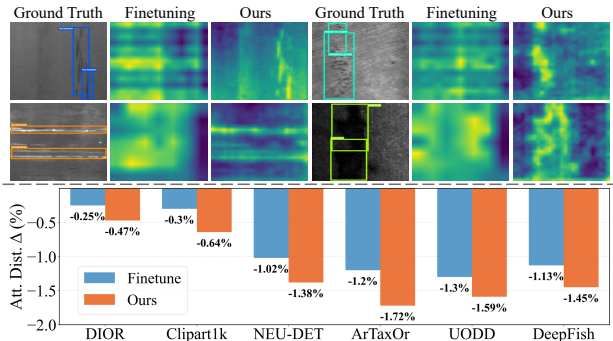


Figure 5. **Top:** Visualization of attention maps demonstrating the Astigmatism problem and our solution. Each row displays two different samples: including the original image with ground truth (left), conventional fine-tuning that only marginally alleviates dispersed attention patterns (middle), and ours, which indicates focused attention that precisely concentrates on target regions. **Bottom:** Change in attention distance relative to pretrained model across datasets. Negative values indicate reduction in attention dispersion (larger magnitude means better focus). While fine-tuning reduces dispersion, our method achieves substantially greater reductions, validating our superior ability to address the Astigmatism problem by reshaping attention toward foreground objects.

deliver strong gains on every dataset and shot count, especially Clipart1k and DeepFish, where domain shifts are pronounced, validating that center-periphery attention refinement mitigates cross-domain attention dispersion.

4.3. Ablation Study

Table 5 shows that NCM, PPR, and TSA yield average gains of +1.06%, +2.06%, and +1.59%, respectively, with PPR showing the best improvement on DeepFish, confirming the need for balanced foreground-background modeling.

4.4. Visualization and Analysis

4.4.1. Analysis of Attention Pattern

Figure 5 provides both visual and quantitative evidence of the Attentional Astigmatism problem and our solution’s effectiveness. **Qualitatively**, the top panel shows conventional fine-tuning only marginally alleviates dispersed attention patterns, while our method yields significantly more focused attention that aligns closely with ground truth regions, even for subtle defects in the bottom row examples. **Quantitatively**, the bottom panel shows changes in attention distance relative to the pretrained baseline (negative indicate reduction). While conventional fine-tuning achieves modest reductions (0.25%-1.30%), our approach consistently

achieves larger reductions (0.47%-1.72%) across all datasets, with the most significant improvements on challenging domains like ArTaxOr and DeepFish, validating our superior ability to address the Astigmatism problem.

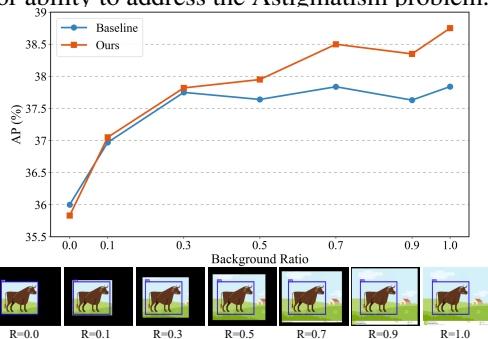


Figure 6. Validation of Negative Context Modulation (NCM) module through background ratio analysis. **Top:** Performance comparison with varying background ratios. Our method demonstrates consistent advantages over the baseline, particularly at higher background ratios (0.3-1.0), indicating NCM exploits negative background contexts as *complementary cues to strengthen foreground feature learning and boundary discrimination*, thereby mitigating the attention dispersion in Astigmatism problem. **Bottom:** Visual examples showing detection with increasing background ratios from left to right (R=0.0 to R=1.0).

4.4.2. Analysis of Background Context Utilization

Figure 6 validates the effectiveness of our Negative Context Modulation (NCM) module in addressing the Astigmatism problem. Both models show comparable performance at low background ratios, but our approach achieves significant gains at higher ratios (0.7-1.0). This performance pattern demonstrates that NCM successfully leverages background contextual information to enhance object-background boundary discrimination. By better utilizing background cues, the model implicitly improves foreground feature learning and localization, thereby easing the attention dispersion issue in cross-domain few-shot detection.

4.4.3. Qualitative Detection Results

Figure 7 demonstrates the effectiveness of our method in alleviating the Astigmatism problem via more focused and compact detections. Our approach consistently produces fewer and more accurate candidate boxes (e.g., reducing from 100 to 9 boxes in maritime scenes) while maintaining precise localization. Across domains, our model avoids false positives from background textures, generates tighter boxes under occlusion, and handles cluttered environments. These results visually confirm that our framework successfully transforms dispersed attention into object-centric focus, directly tackling the attention dispersion in CD-FSOD.

4.5. Parameter Analysis and Discussion

4.5.1. Analysis of Background Text Quantity

Table 6 reveals the impact of background text description quantity on model performance. Gains diminish beyond

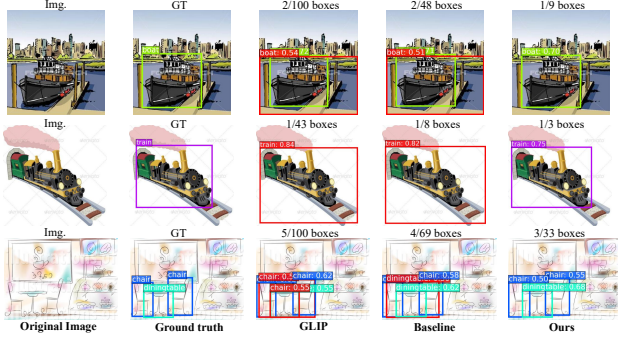


Figure 7. Qualitative detection results on cross-domain scenarios. Our method produces significantly more precise predictions with fewer candidate boxes compared to alternatives. The numbers indicate displayed boxes/total generated boxes, demonstrating our method’s ability to *reduce redundant detections while maintaining precision*. In the maritime scene (top), our approach avoids misclassifying background as objects, while in the transportation (middle) and indoor (bottom) examples, it generates tighter bounding boxes with minimal redundancy. These results validate our framework’s effectiveness in remedying the Astigmatism problem.

Table 6. Effect of background text quantity on performance. Eff. Ratio = $\Delta AP / \Delta Mem.$, indicating AP gain per MB increase.

Text Count	Performance		GPU Mem. (MB) ↓	Eff. Ratio ↑
	AP (%) ↑	Gain ↑		
50	39.34	-	8762	-
100	40.31	+0.97%	8850	1.10%
150	41.48	+1.17%	8943	1.26%
200	42.87	+1.39%	9027	1.65%
250	43.47	+0.60%	9108	0.74%
300	43.80	+0.33%	9178	0.47%
350	43.97	+0.17%	9217	0.44%
400	44.05	+0.08%	9245	0.29%

200 descriptions—the largest increment occurs from 150 to 200 descriptions (+1.39%), with diminishing returns thereafter (+0.08% at 400 descriptions). Therefore, 200 descriptions provides the optimal performance-efficiency trade-off. Notably, our complete framework introduces minimal **computational overhead** with negligible additional parameters and modest memory increases, demonstrating excellent deployment efficiency (detailed analysis in Appendix).

4.5.2. Analysis of Background Alignment Loss Weight

Figure 8(left) demonstrates the impact of TSA loss weight on our approach’s effectiveness. The optimal performance occurs at $\lambda = 10^3$, showing substantial improvement over baseline, which confirms that the TSA strengthens the distinctions between center and peripheral regions. The performance drop at extreme values validates our design principle that balanced cross-modal alignment is essential—neither insufficient nor excessive background emphasis yields optimal results. This supports our framework’s ability to transform dispersed attention patterns into focused object-centric features through calibrated textual-visual feature alignment.

4.5.3. Analysis of Negative Feature Threshold

Figure 8(right) shows the effect of threshold selection in the Negative Context Modulation module. Our method

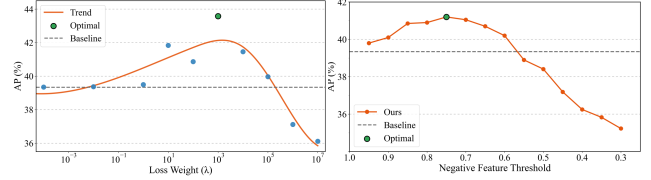


Figure 8. Analysis of key parameters in our approach. **Left:** Effect of TSA loss weight (λ) on detection performance. Performance remains stable when $\lambda \leq 1$, peaks at $\lambda = 10^3$, and declines beyond that, underscoring the importance of appropriate weighting in enhancing object-background separation. **Right:** Impact of threshold selection on NCM effectiveness. Performance remains above baseline across a wide threshold range (0.6-0.9), with optimal results at 0.75, demonstrating that selectively enhancing background features effectively reinforces object-background boundaries.

consistently surpasses the baseline over a wide threshold range (0.6–0.9), with high thresholds still improving performance—indicating that updating a small portion of background features strengthens object–background separation. Performance peaks at 0.75, while lower thresholds risk degrading features due to excessive modification, confirming that targeted background enhancement effectively alleviates astigmatism without large-scale feature changes.

4.5.4. Temperature and Weight Analysis in PPR

Figure 9 shows the interaction between temperature and weight parameters in our PPR module. Moderate weights (0.1–1.0) consistently outperform extremes, with performance dropping sharply above 1.0. This supports our design principle that excessive foreground enhancement harms attention refinement. Robust performance across a wide temperature range within the optimal weight zone demonstrates the PPR module’s robustness across domains.

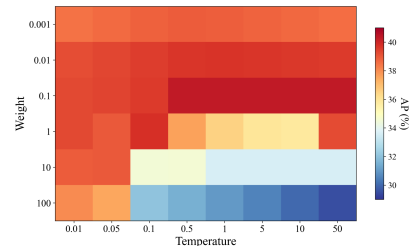


Figure 9. Parameter analysis of temperature-weight interactions in PPR. The heatmap shows peak performance at moderate weights (0.1-1.0) with robust temperature tolerance, while extreme weights (≥ 1.0) cause significant performance degradation. This confirms that balanced prototype utilization is essential for effective attention refinement without disrupting original feature representations.

5. Conclusion

We identified the Astigmatism problem in CD-FSOD, where models exhibit dispersed attention in target domains, and proposed a comprehensive center-periphery attention refinement framework. Experiments demonstrate significant improvements over state-of-the-art methods.

Acknowledgments

This work is supported by the National Natural Science Foundation of China under grants 62206102; the National Key Research and Development Program of China under grant 2024YFC3307900; the National Natural Science Foundation of China under grants 62436003, 62376103 and 62302184; Major Science and Technology Project of Hubei Province under grant 2025BAB011 and 2024BAA008; Hubei Science and Technology Talent Service Project under grant 2024DJC078; and Ant Group through CCF-Ant Research Fund. The computation is completed in the HPC Platform of Huazhong University of Science and Technology.

References

- [1] Mihalj Bakator and Dragica Radosav. Deep learning and medical diagnosis: A review of literature. *Multimodal Technologies and Interaction*, 2(3), 2018. 1
- [2] Xiaozhi Chen, Huimin Ma, Ji Wan, Bo Li, and Tian Xia. Multi-view 3d object detection network for autonomous driving. In *Proceedings of the IEEE Conference on Computer Vision and Pattern Recognition*, pages 1907–1915, 2017. 1
- [3] Geir Drange. Arthropod taxonomy orders object detection dataset, 2020. 6
- [4] Andre Esteva, Katherine Chou, Serena Yeung, Nikhil Naik, Ali Madani, Ali Mottaghi, Yun Liu, Eric Topol, Jeff Dean, and Richard Socher. Deep learning-enabled medical computer vision. *NPJ digital medicine*, 4(1):5, 2021. 1
- [5] Yuqian Fu, Yu Wang, Yixuan Pan, Lian Huai, Xingyu Qiu, Zeyu Shanguan, Tong Liu, Yanwei Fu, Luc Van Gool, and Xingqun Jiang. Cross-domain few-shot object detection with enhanced open-set object detector. In *European Conference on Computer Vision*, pages 247–264. Springer, 2024. 1, 2, 3, 5, 6
- [6] Yipeng Gao, Lingqiao Yang, Yunchao Huang, Shupeng Xie, Shoukui Li, and Wei-Shi Zheng. AcrofoD: An adaptive method for cross-domain few-shot object detection. In *European Conference on Computer Vision (ECCV)*, pages 673–690, 2022. 3
- [7] Yipeng Gao, Kun-Yu Lin, Jingdong Yan, Yingwei Wang, and Wei-Shi Zheng. Asyfod: An asymmetric adaptation paradigm for few-shot domain adaptive object detection. In *Proceedings of the IEEE/CVF Conference on Computer Vision and Pattern Recognition*, pages 3261–3271, 2023. 2
- [8] Naoto Inoue, Ryosuke Furuta, Toshihiko Yamasaki, and Kiyoharu Aizawa. Cross-domain weakly-supervised object detection through progressive domain adaptation, 2018. 6
- [9] Naoto Inoue, Ryosuke Furuta, Toshihiko Yamasaki, and Kiyoharu Aizawa. Cross-domain weakly-supervised object detection through progressive domain adaptation. In *Proceedings of the IEEE Conference on Computer Vision and Pattern Recognition*, pages 5001–5009, 2019. 3
- [10] Lihao Jiang, Yi Wang, Qi Jia, Shengwei Xu, Yu Liu, Xin Fan, Haojie Li, Risheng Liu, Xinwei Xue, and Ruili Wang. Underwater species detection using channel sharpening attention. In *Proceedings of the 29th ACM International Conference on Multimedia*, page 4259–4267, New York, NY, USA, 2021. Association for Computing Machinery. 6
- [11] Yongwei Jiang, Yixiong Zou, Yuhua Li, and Ruixuan Li. Revisiting pool-based prompt learning for few-shot class-incremental learning. In *Proceedings of the IEEE/CVF International Conference on Computer Vision*, pages 1303–1313, 2025. 3
- [12] Ying Jin, Jinlong Peng, Qingdong He, Teng Hu, Hao Chen, Jiafu Wu, Wenbing Zhu, Mingmin Chi, Jun Liu, Yabiao Wang, et al. Dualanodiff: Dual-interrelated diffusion model for few-shot anomaly image generation. *arXiv preprint arXiv:2408.13509*, 2024. 3
- [13] Jochen Laubrock, Anke Cajar, and Ralf Engbert. Control of fixation duration during scene viewing by interaction of foveal and peripheral processing. *Journal of Vision*, 13(12): 11–11, 2013. 2
- [14] Ke Li, Gang Wan, Gong Cheng, Liqiu Meng, and Junwei Han. Object detection in optical remote sensing images: A survey and a new benchmark. *ISPRS Journal of Photogrammetry and Remote Sensing*, 159:296–307, 2020. 6
- [15] Liunian Harold Li, Pengchuan Zhang*, Haotian Zhang*, Jianwei Yang, Chunyuan Li, Yiwu Zhong, Lijuan Wang, Lu Yuan, Lei Zhang, Jenq-Neng Hwang, Kai-Wei Chang, and Jianfeng Gao. Grounded language-image pre-training. In *CVPR*, 2022. 5, 6
- [16] Yanghao Li, Hanzi Mao, Ross Girshick, and Kaiming He. Exploring plain vision transformer backbones for object detection. *arXiv preprint arXiv:2203.16527*, 2022. 5, 6
- [17] Yu Li, Xingyu Qiu, Yuqian Fu, Jie Chen, Tianwen Qian, Xu Zheng, Danda Pani Paudel, Yanwei Fu, Xuanjing Huang, Luc Van Gool, and Yu-Gang Jiang. Domain-rag: Retrieval-guided compositional image generation for cross-domain few-shot object detection, 2025. 5, 6
- [18] Tsung-Yi Lin, Michael Maire, Serge Belongie, Lubomir Bourdev, Ross Girshick, James Hays, Pietro Perona, Deva Ramanan, C. Lawrence Zitnick, and Piotr Dollár. Microsoft coco: Common objects in context, 2015. 3
- [19] Chang-Han Liu, Xunzhi Xiang, Zixuan Duan, Wenbin Li, Qi Fan, and Yang Gao. Don’t need retraining: A mixture of detr and vision foundation models for cross-domain few-shot object detection. In *The Thirty-ninth Annual Conference on Neural Information Processing Systems*. 5, 6
- [20] Boyuan Meng, Xiaohan Zhang, Peilin Li, Zhe Wu, Yiming Li, Wenkai Zhao, Beinan Yu, and Hui-Liang Shen. Cd-former: Cross-domain few-shot object detection transformer against feature confusion, 2024. 3
- [21] Maithra Raghu, Thomas Unterthiner, Simon Kornblith, Chiyuan Zhang, and Alexey Dosovitskiy. What do self-supervised vision transformers learn? In *International Conference on Learning Representations (ICLR)*, 2023. 2
- [22] Alzayat Saleh, Issam H. Laradji, Dmitry A. Kononov, Michael Bradley, David Vazquez, and Marcus Sheaves. A realistic fish-habitat dataset to evaluate algorithms for underwater visual analysis. *Scientific Reports*, 10(1), 2020. 6

- [23] Yijun Shi, Jiaojiao Li, Yunsong Li, Qian Du, Wei Liu, and Jun Zhu. Sensor-independent hyperspectral target detection with semisupervised domain adaptive few-shot learning. *IEEE Transactions on Geoscience and Remote Sensing*, 59(8):6894–6906, 2020. 3
- [24] Jimmy Singla, Kaustubh Arun Bhavsar, Yasser D. Al-Otaibi, Oh-Young Song, Yousaf Bin Zikria, and Ali Kashif Bashir. Medical diagnosis using machine learning: A statistical review. *Computers, Materials & Continua*, 67(1):107–125, 2021. 1
- [25] Kechen Song and Yunhui Yan. A noise robust method based on completed local binary patterns for hot-rolled steel strip surface defects. *Applied Surface Science*, 285:858–864, 2013. 6
- [26] Emma EM Stewart, Matteo Valsecchi, and Alexander C Schütz. A review of interactions between peripheral and foveal vision. *Journal of vision*, 20(12):2–2, 2020. 2
- [27] Domen Tabernik, Samo Šela, Jure Skvarč, and Danijel Skočaj. Segmentation-based deep-learning approach for surface-defect detection. *Journal of Intelligent Manufacturing*, 31:759–776, 2020. 1
- [28] Tao Wang, Xiaopeng Zhang, Li Yuan, and Jiashi Feng. Few-shot adaptive faster r-cnn. In *Proceedings of the IEEE/CVF Conference on Computer Vision and Pattern Recognition (CVPR)*, pages 7166–7175, 2019. 3
- [29] Xu Wang, Cheng Li, Yi Chang, Jindong Wang, and Yuan Wu. Negativeprompt: Leveraging psychology for large language models enhancement via negative emotional stimuli, 2024. 3
- [30] Zhengyang Wang, Tingliang Feng, Fan Lyu, Fanhua Shang, Wei Feng, and Liang Wan. Dual semantic guidance for open vocabulary semantic segmentation. In *Proceedings of the IEEE/CVF Conference on Computer Vision and Pattern Recognition (CVPR)*, 2025. 3
- [31] Katharina Weiß, Werner X Schneider, and Arvid Herwig. Associating peripheral and foveal visual input across saccades: A default mode of the human visual system? *Journal of Vision*, 14(11):7–7, 2014. 2
- [32] Wuti Xiong. Cd-fsod: A benchmark for cross-domain few-shot object detection. In *ICASSP 2023 - 2023 IEEE International Conference on Acoustics, Speech and Signal Processing (ICASSP)*, pages 1–5, 2023. 5, 6
- [33] Wei Xiong. Cd-fsod: A benchmark for cross-domain few-shot object detection. In *Proceedings of the IEEE International Conference on Acoustics, Speech and Signal Processing (ICASSP)*, 2023. 1, 3
- [34] Mengran Yuan, Chenglong Cai, Tongyang Lu, Xudong Zhou, and Pengbo Yan. A novel forget-update module for few-shot domain generalization. *Pattern Recognition*, 129:108704, 2022. 3
- [35] Lin Zhang, Bo Zhang, Botian Shi, Jiayuan Fan, and Tao Chen. Few-shot cross-domain object detection with instance-level prototype-based meta-learning. *IEEE Transactions on Circuits and Systems for Video Technology*, 34(10):9078–9089, 2024. 3
- [36] Xiang Zhang, Yutong Liu, Xuejing Chen, Shilong Sun, Lei Zhang, Heng Fan, Yuyin Chen, Weidi Xie, Xingyi Zhou, Liangzhe Yuan, Xiaoshuai Li, Chenchen Zhao, and Dahua Lin. Detect everything with few examples. In *Conference on Robot Learning (CoRL)*, 2024. 5, 6
- [37] Zhenyu Zhang, Guangyao Chen, Yixiong Zou, Zhimeng Huang, Yuhua Li, and Ruixuan Li. Micm: Rethinking unsupervised pretraining for enhanced few-shot learning. In *Proceedings of the 32nd ACM International Conference on Multimedia*, pages 7686–7695, 2024. 3
- [38] Zhenyu Zhang, Guangyao Chen, Yixiong Zou, Yuhua Li, and Ruixuan Li. Learning unknowns from unknowns: Diversified negative prototypes generator for few-shot open-set recognition. In *Proceedings of the 32nd ACM International Conference on Multimedia*, pages 6053–6062, 2024.
- [39] Zhenyu Zhang, Guangyao Chen, Yixiong Zou, Zhimeng Huang, and Yuhua Li. Decoupling template bias in clip: Harnessing empty prompts for enhanced few-shot learning. *arXiv preprint arXiv:2512.08606*, 2025.
- [40] Zhenyu Zhang, Guangyao Chen, Yixiong Zou, Yuhua Li, and Ruixuan Li. Reclaiming lost text layers for source-free cross-domain few-shot learning. *arXiv preprint arXiv:2603.05235*, 2026. 3
- [41] Zhenyu Zhang, Yixiong Zou, Yuhua Li, Ruixuan Li, and Guangyao Chen. Mind the discriminability trap in source-free cross-domain few-shot learning. *arXiv preprint arXiv:2603.13341*, 2026. 3
- [42] An Zhao, Mingyu Ding, Zhiwu Lu, Tao Zhang, Jihao Xiang, Yao Niu, Makoto Yamada, and Yi Chang. Domain-adaptive few-shot learning. In *Proceedings of the IEEE/CVF Winter Conference on Applications of Computer Vision*, pages 1390–1399, 2021. 3
- [43] Yaze Zhao, Yixiong Zou, Yuhua Li, and Ruixuan Li. Interpretable cross-domain few-shot learning with rectified target-domain local alignment. *arXiv preprint arXiv:2603.17655*, 2026. 3
- [44] Xiaoqing Zheng, Song Zheng, Yaguang Kong, and Jie Chen. Recent advances in surface defect inspection of industrial products using deep learning techniques. *The International Journal of Advanced Manufacturing Technology*, 113(1):35–58, 2021. 1
- [45] Chenfan Zhong, Junran Wang, Chen Feng, Yansong Zhang, Jianmin Sun, and Yoshiyuki Yokota. Pica: Point-wise instance and centroid alignment based few-shot domain adaptive object detection with loose annotations. In *Proceedings of the IEEE/CVF Winter Conference on Applications of Computer Vision (WACV)*, pages 2329–2338, 2022. 3
- [46] Xingyi Zhou, Rohit Girdhar, Armand Joulin, Philipp Krähenbühl, and Ishan Misra. Detecting twenty-thousand classes using image-level supervision. In *ECCV*, 2022. 5, 6
- [47] Yixiong Zou, Shanghang Zhang, Yuhua Li, and Ruixuan Li. Margin-based few-shot class-incremental learning with class-level overfitting mitigation. *Advances in neural information processing systems*, 35:27267–27279, 2022. 3
- [48] Yixiong Zou, Yicong Liu, Yiman Hu, Yuhua Li, and Ruixuan Li. Flatten long-range loss landscapes for cross-domain few-shot learning. In *Proceedings of the IEEE/CVF Conference on Computer Vision and Pattern Recognition*, pages 23575–23584, 2024.

- [49] Yixiong Zou, Ran Ma, Yuhua Li, and Ruixuan Li. Attention temperature matters in vit-based cross-domain few-shot learning. *Advances in Neural Information Processing Systems*, 37:116332–116354, 2024.
- [50] Yixiong Zou, Shuai Yi, Yuhua Li, and Ruixuan Li. A closer look at the cls token for cross-domain few-shot learning. *Advances in Neural Information Processing Systems*, 37: 85523–85545, 2024.
- [51] Yixiong Zou, Shanghang Zhang, Haichen Zhou, Yuhua Li, and Ruixuan Li. Compositional few-shot class-incremental learning. *arXiv preprint arXiv:2405.17022*, 2024. [3](#)